20th Australasian Fluid Mechanics Conference
Perth, Australia
5-8 December 2016

Gravity Current Propagation through Fields of Roughness Elements

R. Nokes[1], C. Cenedese[2] , M. Ball[1] and T. Williams[1]

[1]Department of Civil and Natural Resources Engineering
University of Canterbury, Christchurch 8140, New Zealand

[2]Department of Physical Oceanography
Woods Hole Oceanographic Institution, Woods Hole, Massachusetts MA02543-1050, USA

Abstract

The interaction of gravity currents with significant boundary roughness is a relatively unexplored field of research. Results from an experimental campaign aimed at exploring the impact of roughness configuration and relative roughness height on the dynamics of a dense boundary gravity current are presented. A PTV system provides detailed velocity field data for gravity currents created using a standard lock exchange configuration and flowing through a roughness field of vertical circular cylinders. Particular attention is paid to the general flow regimes observed and the dependence of the Froude number of the current front, *Fr*, on the roughness field characteristics. It is demonstrated that it is possible that increasing roughness density can lead, first, to a decrease in *Fr* and then to an increase.

Introduction

Gravity currents, flows driven by horizontal gradients in fluid density, are common in geophysical fluid systems. Simpson [4] provides both an excellent introduction to the wide variety of circumstances in which these currents can appear in the environment as well as a thorough description of the fundamental dynamics of these flows.

Despite the fact that there is a significant research literature related to gravity currents little work has focussed on the geophysically important problem of the interaction of boundary currents with roughness fields where individual roughness elements have a height that is comparable with the depth of the current itself. Examples of such flows in the environment include turbidity currents and oceanic overflows interacting with bottom roughness and atmospheric flows encountering buildings.

Nepf and her collaborators have made significant contributions to understanding a closely related problem of fluid flow through canopies of various types [2, 5].

The research presented here is part of a larger investigation into the dynamics of currents encountering large roughness fields, with a particular focus on entrainment, mixing, flow structure and front propagation speed. In this paper we limit our attention to the impact of a longitudinal variation in roughness configuration.

Methodology

Flume

A standard lock-exchange configuration was used to generate a dense gravity current in a horizontal flume measuring 6.2m (L) × 0.5m (H) × 0.25m (W) (see figure 1). The flume was constructed of clear Perspex sheets to enable flow visualisation through the flume walls. A sealed, vertical, stainless steel gate located 1m from the right hand end of the flume, partitioned the flume into two compartments. In the larger of the two compartments a field of roughness elements was constructed from an array of 5cm high and 2cm diameter plastic cylinders, with vertical axes,

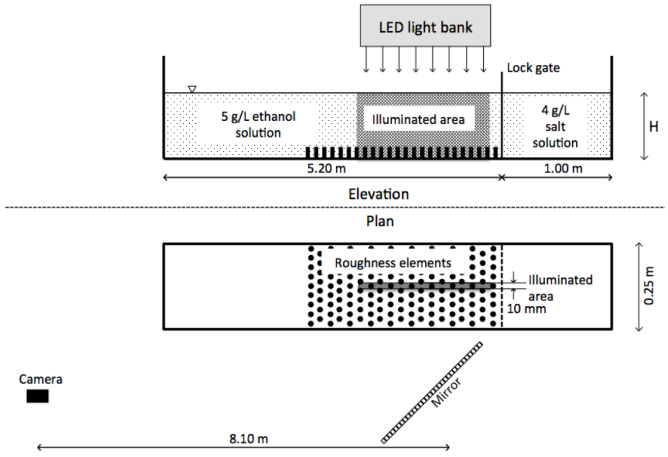

Figure 1. Elevation and plan views of the experimental flume and optical system components.

screwed into an aluminium base plate. The configuration of the roughness elements was easily varied by adding or removing cylinders. This roughness field extended 3m from the gate.

Three non-dimensional geometric parameters characterise the layout of the cylinders. The definitions of these parameters is not unique and, for convenience, we have chosen the following parameters: The *plan density*, σ, is defined by

$$\sigma = \frac{A_P}{A_{TP}} \tag{1}$$

where A_P is the area of the base covered by the cylinders in plan and A_{TP} is the total area of the base in plan. The *elevation density*, μ, is defined by

$$\mu = \frac{A_E}{A_{TE}} \tag{2}$$

where A_E is the area of the field covered by the cylinders in elevation as seen by the advancing current and A_{TE} is the total area of the field in elevation (measured to the top of the cylinders). And finally the *aspect ratio*, α, is defined by

$$\alpha = \frac{h}{d} \tag{3}$$

where h is the height of the cylinders, and d is their diameter.

Figure 2 illustrates the three roughness arrangements used in this study. They correspond to α = 2.5, μ = 0.64 and σ taking the values of 0.045, 0.09 and 0.18.

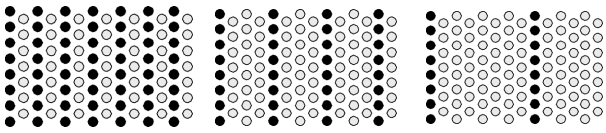

(a) (b) (c)

Figure 2. Plan view of the three roughness configurations. (a) σ=0.18 (b) σ = 0.09 (c) σ = 0.045. Dark circles indicate occupied cylinder locations and grey circles indicate unoccupied locations.

Initial Conditions

Two fluids with matching refractive indices, but differing densities, were prepared before the start of each experiment. The denser saltwater solution filled the lock region while the less dense ethanol solution filled the remainder of the flume. To ensure Boussinesq behaviour a density difference of approximately 0.5% was selected – the exact density being measured with an Anton Parr DMA5000 density meter.

The height of the fluid in the flume, H, relative to the roughness height, provided a further dimensionless parameter related to the initial conditions. The *depth ratio* is defined to be

$$\lambda = \frac{h}{H} \tag{4}$$

λ took values of 0.14, 0.19, 0.25 and 0.33 for each value of σ and these values corresponded to water depths of 350mm, 270mm, 200mm and 150mm respectively.

Particle Tracking System

A particle tracking velocimetry (PTV) system was employed to measure the flow structure in each of the experiments. Prior to the commencement of an experiment both fluids were seeded with pliolite particles (of density 1.03 g/cm^3) in the range 250-300μm. These particles were illuminated by a bespoke white light-sheet generator comprising a linear sequence of high intensity LEDs located above the working section of the flume (see figure 1). Subsequent to the removal of the gate a JAI BB141GE video camera recorded 1392×1040 pixel images of the particle motion at a frame rate of approximately 30Hz. The matched refractive indices of the two fluids ensured undistorted images of the particles were captured. To reduce parallax errors the camera was mounted alongside the flume and the motion was viewed through a mirror angled at 45° to the light path (see figure 1).

All image processing was undertaken with the *Streams* software system [3]. The final output from this analysis was a non-dimensional 2D velocity field translated into the frame of reference of the front of the gravity current. The dimensionless variables utilised in this final representation of the data were

$$x' = \frac{x}{H}, \qquad y' = \frac{y}{H} \tag{5}$$

$$u' = \frac{u}{U_f}, \qquad v' = \frac{v}{U_f} \tag{6}$$

where x and y are the horizontal and vertical coordinates respectively with the origin set to be on the flume bottom directly beneath the stagnation point at the nose of the current, u and v are the horizontal and vertical velocity components, and U_f is the front speed of the current.

Determination of the front speed of a gravity current using velocity field data is not straightforward. A number of different methods, utilising both the velocity field and the raw particle data, were used to provide estimates of the front speed and the spread in these estimates provided the error bars presented in figure 8.

A parameter of prime importance is the dimensionless front speed, the Froude number, Fr, defined to be

$$Fr = \frac{U_f}{\sqrt{g'H}} \tag{7}$$

where the reduced gravity, g' is defined to be

$$g' = g\left(\frac{\rho_s - \rho_e}{\rho_e}\right) \tag{8}$$

where g is the acceleration due to gravity, and ρ_s and ρ_e are the initial densities of the salt and ethanol solutions respectively.

Data Quality

The two-dimensional velocity fields reported here suffer from two intrinsic limitations. Firstly, in order to obtain meaningful time-averaged statistics it must be assumed that the current, during its early evolution, is in a quasi steady state regime such that the front speed of the current does not change appreciably during the recorded motion and the internal flow is statistically stationary in the frame of reference of the current front. Thus our final velocity fields are treated as being in steady state. Secondly, the time available for averaging the turbulent fluctuations within the current is limited. While each experiment may last in excess of 30 seconds the period of time over which a part of the current is visible to the camera, as it passes through the camera's field of view, is significantly less than this. Thus the Reynolds averages are not exact.

Figures 3 provides some insight into the severity of these issues. In this figure vertical profiles of the horizontal velocity at x' = -1 are plotted for three repeat experiments with the same initial conditions. The variability between these profiles is reflective of the two issues discussed above as well as the difficulty in identifying the stagnation point for each flow (which determines the location of x' = 0). The Froude numbers for these 3 repeats were 0.27 ± 0.01.

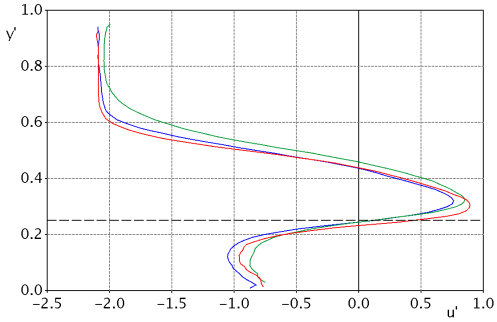

Figure 3. Vertical profile of u' at x' = -1 (one fluid depth behind the current nose) for σ = 0.18 and λ = 0.25 for three repeats of the same experiment. The horizontal dashed black line is the roughness height.

Results

Flow Regimes

The flow regimes observed in these experiments varied significantly. They are, perhaps, most easily understood by considering the two extreme cases of σ = 0 and σ = 1. The first of these corresponds to the smooth bed case and the gravity current takes the form of a standard, smooth boundary current. The second also corresponds to a smooth bed as, in this case, the

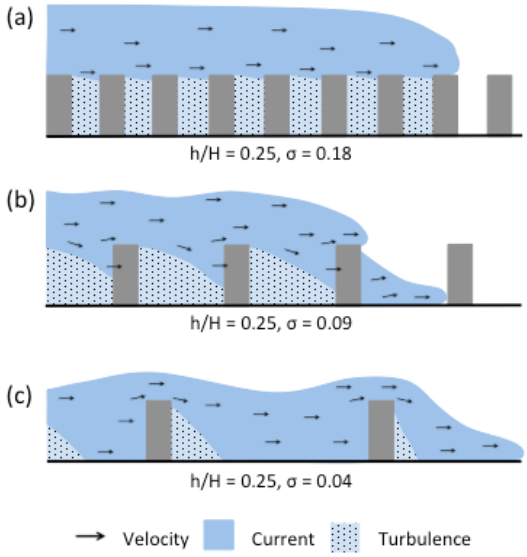

Figure 4. Schematics of the flow structure for fixed $\lambda = 0.25$ and variable σ (a) $\sigma = 0.18$ (b) $\sigma = 0.09$ (c) $\sigma = 0.04$.

roughness elements contain no voids. Thus the current will sit atop the roughness elements and take the same form as for the $\sigma = 0$ case. It is worth noting that the limit of $\sigma = 1$ is not possible for all roughness element arrangements. For example the most closely packed cylinders will still possess gaps between the cylinders. In addition, irrespective of the roughness element cross-section, the maximum possible value of σ is limited to less than or equal to μ.

Between these two roughness limits the current gradually transitions from propagating along the bottom of the flume to propagating along the top of the roughness elements. From our observations the flow could be broadly categorised into three regimes. These are illustrated by the cartoons in figure 4. For large roughness densities the presence of the roughness elements forces the current to flow predominantly above the obstacles (figure 4(a)). As discussed by Cenedese et al [1] these flows are strongly modified by the buoyant exchange between current fluid and the ambient fluid trapped between the elements. The fluid denoted "Turbulence" in the figure is undergoing turbulent convective motion. As the roughness density decreases the body of the current shifts progressively downwards until the bulk of the current lies within the roughness field. For the smallest value of σ the current resembles a smooth boundary current that occasionally encounters a row of obstacles. While some fluid passes between the elements much of the current mounts the obstacles and flows over them (figure 4(c)). The regions denoted "Turbulence" in figures 4(b) and (c) correspond to turbulent wake regions behind the cylinders.

Quantitative differences between these flow regimes are illustrated by the vertical profiles of horizontal velocity in figure 5. The profiles are located one flow depth behind the current nose in the steady reference frame. For the greatest roughness density the current is perched higher in the flume with the result that the ambient flow above the current has a higher velocity than for the lower densities. The flow within the roughness elements is almost stationary in the laboratory frame and the impact of this flow restriction is to generate larger velocities towards the nose within the current itself. As the roughness density decreases the fluid between the elements begins to move increasingly with the current and thus the velocity within the current reduces. The downward shift in the current bulk is also clear in the figure.

Figures 6(a) and (b) provide further evidence of the difference in flow structure within the roughness elements. These two figures

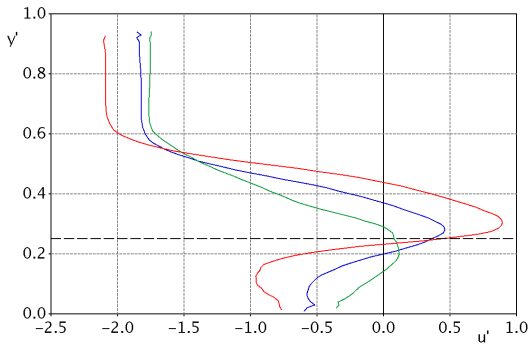

Figure 5. Vertical profiles of u' at $x' = -1$ for the same parameters as figure 4. Red - $\sigma = 0.18$, blue - $\sigma = 0.09$, green - $\sigma = 0.04$ .The horizontal dashed black line is the roughness height.

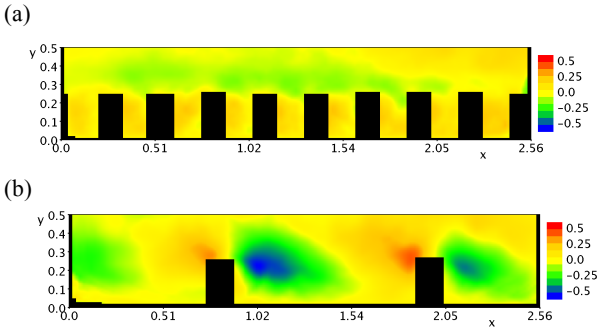

Figure 6. Colour plots of the time-averaged vertical velocity in the laboratory frame of reference for fixed $\lambda = 0.25$ and variable σ (a) $\sigma = 0.18$ (b) $\sigma = 0.04$.

have been produced by time-averaging the vertical velocity field in the laboratory frame of reference after the current nose has passed. While this averaging process is not a true Reynolds average, as the flow is not steady, it does illustrate the point that the current tends to flow atop the roughness elements for high roughness densities while for low densities the current flows up and over the rows of elements.

The same flow regimes as illustrated in figure 4 also appear when the depth ratio, h/H, is varied. For fixed roughness density the current tends to flow above the elements as the depth ratio decreases (i.e. as the current becomes deeper). A series of cartoons are provided in figure 7 to illustrate these changes.

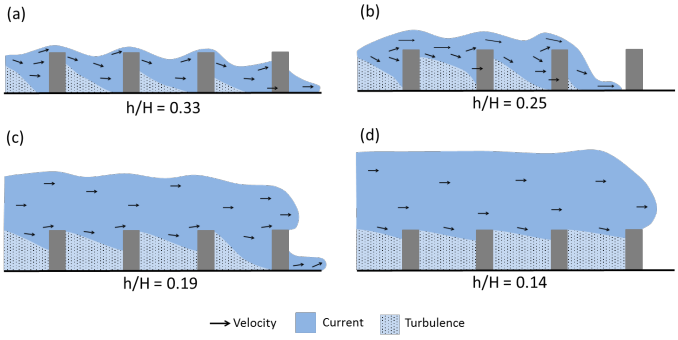

Figure 7. Schematics of the flow structure of for fixed $\sigma = 0.09$ and variable λ (a) $\lambda = 0.33$, (b) $\lambda = 0.25$, (c) $\lambda = 0.19$ (d) $\lambda = 0.14$.

Froude Number

A primary parameter of interest for all gravity current flows is their speed of advance, or, in dimensionless form, their Froude number, as defined in equation (7). Figure 8 presents the *Fr* for each of the flows considered in this study along with a number of additional results taken from [1]. These additional results include those for a smooth bed current as well as those for a higher roughness density than covered in the experiments reported here. The first of these yielded a *Fr* of 0.46 and, provided the Reynolds number was large enough and the current was fully turbulent, this value was independent of the scale of the current. The second corresponds to $\sigma = 0.33$. However these latter results must be treated with some caution as the μ value for these experiments does not match that used in the current study. The roughness field, in this case, was produced by populating all of the cylinder locations illustrated in figure 2.

The data in the figure provide a number of insights into the impact of a roughness field on the gravity current speed. Firstly, for fixed roughness layout, the Froude number decreases with increasing depth ratio (i.e. the current scale reduces relative to the roughness height). The reason for this behaviour is twofold. Firstly, the drag experienced by the current is relatively more significant for shallower currents than for deeper currents. Secondly, and probably most importantly, deeper currents tend to flow above the roughness field, as illustrated in figure 7.

Similarly *Fr* is seen to decrease with increasing roughness density, at least until $\sigma = 0.1$. However there is strong evidence that this trend does not continue ad infinitum. The data suggest that for each value of λ there exists a value of σ at which *Fr* is a minimum. While the data in figure 8 is incomplete it does indicate that σ_{min} increases with increasing λ. This is consistent with the previous observation that currents with smaller depth ratio transition to the overriding flow regime earlier than those with larger depth ratios and hence the apparent reduction in drag happens earlier for these deeper currents. This conclusion is also consistent with the argument, presented earlier, that the current ultimately returns to being a smooth boundary current, albeit with a slightly reduced value of *H*, as σ tends towards 1.

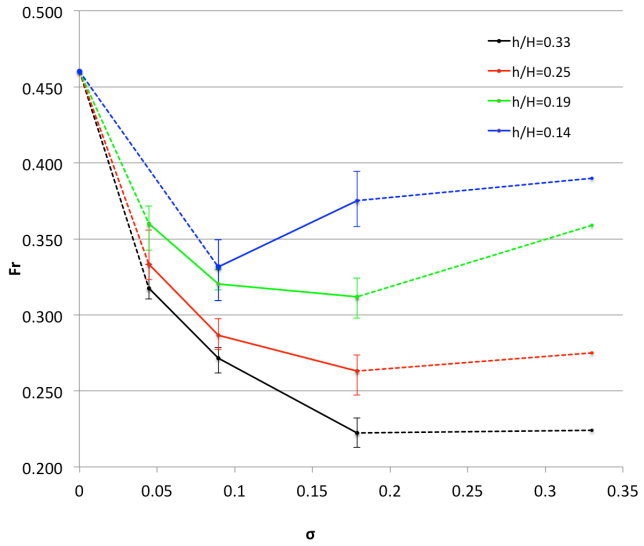

Figure 8. Fr dependence on σ, including data from [1] for σ = 0 and σ = 0.33. The solid lines are linear interpolations between the data from this study while the dashed lines interpolate between the data from this study and that of [1].

This result, that a gravity current may actually flow faster as the roughness that it encounters increases in density, while counter-intuitive, is based on sound physical arguments.

Conclusions

We have presented results from an experimental study of gravity currents encountering a field of roughness elements of varying density and depth ratios. All roughness configurations took the form of regular, cross-stream rows of vertical circular cylinders where the change in roughness density was achieved by removing rows of cylinders. The flows were analysed using a particle tracking velocity system fixed in the laboratory frame of reference.

The key results can be summarised as follows:

1. A number of flow regimes were observed, most easily understood by considering two extremes. In one extreme, where the roughness elements are packed close together, the current rides on top of the roughness elements and approximates a smooth boundary current in the limit as the roughness elements cover the entire lower boundary. In the other extreme the roughness elements are sparsely distributed on the lower boundary and the current acts as a smooth boundary current occasionally encountering a row of cylinders that must be negotiated – typically by primarily flowing over the cylinders for the configurations considered here.

2. Between these two extremes the current adopts a structure whereby some portion of the current lies within the roughness elements while the remainder lies above. As the roughness density increases or the depth ratio decreases the flow transitions from the flow-through regime to the overriding regime.

3. As the roughness density increases the *Fr* of the current initially decreases, but after some value of the plan density, σ, dependent on the depth ratio, λ, the *Fr* will again increase as it approaches the high roughness density limit.

Acknowledgments

The authors wish to express their thanks to Ian Sheppard and Kevin Wines for their invaluable technical support. This project was partially funded by NSF Grant OCE-1333174.

References

[1] Cenedese, C., Nokes, R. & Hyatt, J., Mixing in a density-driven current flowing over a rough bottom. *20th AFMC.* Perth Australia, December 2016.

[2] Nepf, H., Flow and transport in regions with aquatic vegetation, *Annual Review of Fluid Mechanics*, **44**, 2012 123-142.

[3] Nokes, R., *Streams 2.05 – System Theory and Design*, University of Canterbury, 2016.

[4] Simpson, J., *Gravity currents in the environment and the laboratory*, 2nd Ed., Cambridge University Press, Cambridge, 1997.

[5] Zhang, X. & Nepf, H., Exchange flow between open water and floating vegetation. *Environmental Fluid Mechanics,* **11**, 2011, 531-546.